Published in final edited form as:
ACS Synth Biol. 2013 May 17; 2(5): 255–262. doi:10.1021/sb300093y.

Reverse Engineering Validation using a Benchmark Synthetic Gene Circuit in Human Cells

Taek Kang[1,3], **Jacob T. White**[1,3], **Zhen Xie**[4], **Yaakov Benenson**[5], **Eduardo Sontag**[*,6], and **Leonidas Bleris**[*,1,2,3]

[1]Bioengineering Department, University of Texas at Dallas, 800 West Campbell Road, Richardson TX 75080 USA [2]Electrical Engineering Department, University of Texas at Dallas, 800 West Campbell Road, Richardson TX 75080 USA [3]Center for Systems Biology, University of Texas at Dallas, NSERL 4.708, 800 West Campbell Road, Richardson TX 75080 USA [4]Center for Synthetic and Systems Biology, Bioinformatics Division, TNLIST, 100084, Tsinghua University, Beijing, China [5]Department of Biosystems Science and Engineering, Eidgenössische Technische Hochschule (ETH) Zürich, Mattenstrasse 26, 4058 Basel, Switzerland [6]Department of Mathematics, Rutgers-The State University of New Jersey, Hill Center, 110 Frelinghuysen Rd., Piscataway NJ 08854 USA

Abstract

Multi-component biological networks are often understood incompletely, in large part due to the lack of reliable and robust methodologies for network reverse engineering and characterization. As a consequence, developing automated and rigorously validated methodologies for unraveling the complexity of biomolecular networks in human cells remains a central challenge to life scientists and engineers. Today, when it comes to experimental and analytical requirements, there exists a great deal of diversity in reverse engineering methods, which renders the independent validation and comparison of their predictive capabilities difficult. In this work we introduce an experimental platform customized for the development and verification of reverse engineering and pathway characterization algorithms in mammalian cells. Specifically, we stably integrate a synthetic gene network in human kidney cells and use it as a benchmark for validating reverse engineering methodologies. The network, which is orthogonal to endogenous cellular signaling, contains a small set of regulatory interactions that can be used to quantify the reconstruction performance. By performing successive perturbations to each modular component of the network and comparing protein and RNA measurements, we study the conditions under which we can reliably reconstruct the causal relationships of the integrated synthetic network.

Keywords

Reverse Engineering; Benchmark Synthetic Circuits; Human Cells; Modular Response Analysis

[*]Corresponding authors: L.B. (bleris@utdallas.edu) and E. S. (sontag@math.rutgers.edu).

Author contributions

T. K., L. B., Z. X. performed the experiments. T. K., J. W., L. B. analyzed the data. T. K., L. B., J. W., Y. B., E. S. prepared the manuscript. L. B., E. S., Y. B. conceived the project. L. B. supervised the project.

Notes

The authors declare no competing financial interest.

Supplementary information accompanies this paper. This information is available free of charge via the Internet at http://pubs.acs.org/.

Requests for materials should be addressed to L. B. (bleris@utdallas.edu)

The reverse engineering question has been pursued increasingly since the advent of molecular biology, and the methods have gradually shifted from manual, intuitive pathway reconstructions to high-throughput computational techniques. The latter methods usually consist of collecting experimental data, performing computer-aided data analysis and drawing conclusions, which guide further experiments. A successful implementation of this cycle requires high-quality data, adequate models and algorithms, and confidence that the interpretation is correct. There are many possible issues with the experimental techniques used to generate data and with the algorithmic tools designed to interpret these data, but most importantly, uncertainty stems from our inability to independently verify the conclusions suggested by reverse engineering tools[1,2].

Current reverse engineering (RE) methods differ in every possible dimension of experimental techniques and computational analyses[3, 4, 5]. While each method has demonstrated successful network reconstructions on its own, there are no accepted standards to compare their relative strengths and weaknesses due to major differences in the types of data sets and analyses used. In fact, the lack of unifying standards and procedures for validation, along with the high degree of expertise required for computational algorithms, can be regarded as one of the major obstacles which prevents the widespread use of network inference methods. To address this issue, a community-wide effort, DREAM (Dialogue for Reverse Engineering Assessments and Methods), has been initiated to facilitate discussion and refine existing methodologies, resulting in valuable insights about relationships between algorithm performance and experimental parameters[6, 7, 8].

The assessment and verification of RE algorithms[9, 10] for pathway reconstruction is a critical issue. Results in yeast[11] highlight the usefulness of synthetic circuits for this purpose, but the problem remains largely unsolved in human cells, which are likely the most significant (in terms of the scientific and broader impacts potential) and complex (in terms of the theoretical and experimental issues) platform.

In this paper, we describe an experimental and theoretical procedure to refine and validate biological network inference in human kidney cells. We construct and stably integrate a synthetic gene circuit that resembles a natural network topology, establishing an independent, versatile benchmark system that can assess the performance of a reverse engineering algorithm (Figure 1a). The proposed reverse engineering procedure consists of the following steps. First, a small scale network is stably integrated in mammalian cells. Then, the individual nodes of this network are weakly perturbed from their steady state. The pre- and post-perturbation steady states are measured and fed into a reverse engineering algorithm to predict the network structure. The results of the algorithm are compared against the known network structure, and are used to adjust the parameters of the algorithm and set guidelines for future experiments. These parameters include the perturbation magnitudes, the data collection and processing techniques, and the details of computational processing.

As our baseline reverse engineering method we use an approach based on Modular Response Analysis (MRA), where we take experimentally measured steady-state responses following near-linear perturbation of each modular component of the benchmark system[12, 13, 14]. The criteria for the selection of MRA as “iteration zero” RE method is based on our experience[12, 13, 15] with the method, published experimental work that successfully used the method[16, 17], because it reveals network structure with a relatively simple experiment setup, and importantly due to our conviction that the method is indeed best suited for transitioning from benchmark circuits to endogenous pathways.

We believe that the use of synthetic circuits as benchmarks for reverse engineering has important advantages. First, the synthetic circuits can be engineered to be compatible with

commonly available perturbation (e.g. siRNA or small molecule) and data acquisition (e.g. qRT-PCR or fluorescent microscopy) methods. Furthermore, the versatility and diversity of building blocks for synthetic circuits allows for engineering a wide range of topologies and functions, while being orthogonal to endogenous signaling networks. Once the network is stably integrated in cells and its topology is experimentally confirmed, it can serve as a basis for validating specific aspects of reverse engineering.

Results and Discussion

The benchmark synthetic network

We engineered a synthetic regulatory network that consists of two fluorescent reporters (AmCyan and DsRed) subject to control by two distinct regulatory elements (Figure 1b). Each of the regulatory elements can be controlled by chemical ligands (at a concentration non-toxic to the cell), and their transcriptional products do not interact with endogenous cellular signaling. This simple circuit allows the study of scenarios where the output fluorescent proteins are subject to a range of heterogeneous inputs: no activation, single source of activation, and combination of activation and repression.

The first of the two regulatory units, rtTA, is based on the tetracycline-inducible expression system (Tet-On)[18], and is responsible for initiating transcription of both fluorescent reporters, AmCyan and DsRed, by binding to a bidirectional promoter. The activation of the TRE enhancer by rtTA can be controlled by varying the amount of doxycycline. The second source of regulation is RNA interference in the form of short-hairpin RNA (shRNA). The shRNA was constructed by inserting the FF3 stem-loop in pSiren (Clontech). A gene can be made susceptible to downregulation by an arbitrary miRNA by incorporating targets into its 3'-untranslated region (UTR)[19,20]. By inserting three repeats of FF3 target sequence in the 3' UTR of the DsRed transcript, we down-regulate the expression of the fluorescent protein. The activity of shRNA, which is constitutively transcribed from a U6 promoter, can be modulated by introducing morpholino oligos (GeneTools). The antisense morpholino protects the transcript from degradation by irreversibly binding to the 3' UTR target sequence of DsRed[21, 22].

The expected behavior of the network is best illustrated as a four-node system with three edges. A pair of activation edges from DOX-rtTA node to each fluorescent output node are used in order to indicate doxycycline dependence of the bidirectional promoter, and a third inhibition edge connects the shRNA node to DsRed (Figure 1c). We note here that the input variable morpholino represses the inhibitory effects of shRNA, resulting to an overall positive action on the output, but in reporting the reconstruction results we examine the negative connection between the shRNA and the dsRed protein.

Characterization of the synthetic circuit

The individual parts of the synthetic circuit (Figure 1b) were first cloned into a single vector (Supplemental Information, Cloning) and the cassette was then integrated stably in a FLP-In HEK 293 cell line (Invitrogen). We first examined the behavior of the network in response to titrations of the chemical ligands doxycycline and morpholino (Figure 2). We performed doxycycline titration in the absence of morpholino and morpholino titration for fixed saturated doxycycline concentration (10 μg/ml) (Figure 2a and 2b). The doxycycline concentration ranged from 1 ng/ml to 10 μg/ml, while morpholino concentration ranged from 0 to 5 nmol/ml. All fluorescence microscopy and flow cytometry measurements were performed between 48 to 56 hours after addition of chemical ligands, when the concentration of fluorescent proteins is at quasi-steady state. During the analysis of fluorescence using flow cytometry we discovered that, although stringent selection of cells

positive for the circuit integration was possible, a portion of these cells exhibited leaky transgene expression (Supplement Figure 1). To eliminate this population we include in the analysis only the cells responsive to both input variables by appropriate gating (Supplement Figure 1 and Figure 2). The titrations result in output fluorescent protein measurements consistent with the expected behavior of our network topology. Expression levels of both fluorescent reporters were up-regulated in response to increasing doxycycline. The addition of morpholino results in a significant increase in DsRed intensity but not AmCyan, which indicated that the morpholino successfully interferes with the shRNA function and that the shRNA is indeed responsible for DsRed down-regulation.

Reverse engineering approach

After completing the dose-response profile of the circuit, we attempted to reconstruct the network topology without using our prior knowledge of the circuit. We used a top-down reverse engineering approach to extract interactions from steady-state perturbation experiments. The method is based on modular response analysis[13], and assumes that the biological network is a collection of monotone modules represented by simultaneous output measurements x_i, such as steady state concentrations of protein or mRNA levels. These quantities are thought of as state variables in a dynamical system, which is the set of differential equations, $dx_i/dt = f(x_i, p_i)$ where p_i is a set of input parameters. One introduces coefficients r_{ij} obtained from partial derivatives of f as a measure of pairwise interaction strengths between nodes. The main objective of modular response analysis is to obtain the signs of the pairwise interactions, which represent the nature of the influence exerted by one node onto another. In cases where no interaction exists, r_{ij} should be identified as zero. For our benchmark architecture and in order to obtain the interactions between nodes we have to obtain only the global response coefficients (GRC), obtained experimentally by calculating $\Delta\ln(x_j)$, where x_i represents the steady-state concentration of a state variable, such as protein or mRNA. Once the functional modules (i.e. perturbation targets) of the target network have been selected, the experimental procedure consists of the following steps (Figure 2c): (a) measure the steady-state x_i corresponding to the unperturbed set of inputs p_i, (b) perform a perturbation to each p_i individually and measure the new steady-state, (c) calculate the global response coefficients using the steady-state data. We use the synthetic circuit as a benchmark to validate the reconstruction results and we probe specific perturbation and measurement parameters. First, we examine the impact of the experimental perturbation range on the quality of network reconstruction. Secondly, we probe the consistency of the topology reconstruction between protein (flow cytometry) or mRNA (qRT-PCR) measurements.

Network reconstruction using flow cytometry data

For the first question, we defined a set of perturbation ranges to test the general reconstruction performance. By taking advantage of the dose-dependent dynamics of the circuit, we treated each stepwise decrease in concentration of doxycycline and morpholino during the titration experiment as a perturbation, and obtained the response coefficients for these intervals by calculating the log fractional change in each fluorescence reading (Figure 3). We observed that as doxycycline concentration increases (Figure 3a) the mean fluorescence of AmCyan and DsRed increase. Moreover, morpholino up-regulates DsRed expression. As a single set of complete topology reconstruction consists of the system's response to each input, we took a pair of single-step intervals (annotated in Roman numerals) from each titration data to denote the perturbations, and proceeded with the network reconstruction based on the chosen intervals. In total, we defined six intervals to represent equal numbers of separate perturbation scenarios. The three intervals I through III represent 10-fold increase in doxycycline concentration (starting from 10^0 ng/ml to 10^3 ng/ml), and were used to calculate response coefficients relating Dox-rtTA activity to each of

the fluorescent output nodes (r_{DC} and r_{DR}). Intervals IV through VI represent increase in morpholino concentration (starting from 0 nmol/ml to 1, 3, 5 nmol/ml), and were used to calculate the response coefficients relating the activity of shRNA-FF3-morpholino to the fluorescence output nodes (r_{MC} and r_{MR}). For each set of reconstruction result, intervals were paired based on their relative pre-perturbation concentration for each drug (i.e. I and VI, II and V, III and VI). As a control, we perturbed the fluorescent proteins using siRNA to verify that there is no crosstalk between them (Supplement Figure 2).

In order to estimate the significance of the reconstruction results we calculate the confidence interval of the global response coefficients, and we plot the results using a boxplot showing 2.5 and 97.5 percentiles. More specifically, if the 95% confidence interval does not intersect 0, then the response coefficient is statistically significant, indicating a connection between two nodes. In other words, we only accept calculated coefficients as positive if $P(r_{ij} > 0) > 0.975$ and negative if $P(r_{ij} < 0) > 0.975$.

To generate the confidence interval for the inferred response coefficient using the flow cytometry measurements we selected the method of bootstrap resampling (Methods, Bootstrap)[23]. Briefly, each round of bootstrap estimation consists of: 1) randomly drawing a number N of resamples (with replacement) from flow cytometry data of pre-and post-perturbation states, 2) calculating the mean of fluorescent readings, and 3) performing response coefficient calculation by calculating fractional change $\Delta\ln(x)$ for each protein.

The bootstrap resampling size is a critical parameter as it has an inverse-squared relationship with the size of the confidence interval, which in turn directly affects our conclusions regarding the reconstructed network topology. We select a resampling size such that the variations in the calculated global response coefficients reflect typical experimental errors, and use our knowledge of the benchmark circuit to validate the selection. In particular, for proteins AmCyan and DsRed, we observed the standard errors of 6.5% and 4.4%, respectively (Supplement Table 1). If we select 4.4% as the standard error we obtain a resampling rate of 120 (Methods, Resampling rate selection). When we apply this rate to analyze the results of perturbations outside of protein saturation, the response coefficient representing an edge that is absent (r_{MC}) includes zero in its confidence interval (and thus considered statistically negligible), while all other response coefficient (r_{DC}, r_{DR}, r_{MR}) do not include zero in their 95% confidence interval (Supplement Figure 3). Even when we widen the 95% confidence interval by accepting 6.5 percent standard error and repeating the procedure (N=60), the same topology is retained and identical conclusions can be made.

We proceed to the network reconstruction for the various perturbation scenarios using the resample rate N=120. The confidence interval of the response coefficient was constructed with 1,000 repetitions of bootstrap estimates. For the interval pair III and VI, which represent perturbations applied at or near saturation of both fluorescent proteins, the 95% confidence interval for every response coefficient includes zero, yielding a circuit topology that suggests negligible functional relationship between regulator nodes and output nodes (Figure 3b, top). When we perform the same calculation for the other intervals, we observe that the response coefficients increase in magnitude. Only in a case where no functional relationship exists between two nodes (r_{MC}), the response coefficient show negligible variation in magnitude across all three intervals ($\bar{r}_{MC} = 0.060 \pm 0.034$). Furthermore, we observe a noticeable difference between the response coefficients r_{DC} and r_{DR} despite the fact that rtTA co-regulates AmCyan and DsRed expression via a bidirectional promoter. The comparison of median response coefficients for r_{DR} and r_{DC} indicates that r_{DR} is consistently larger, particularly for higher doxycycline concentration ($r_{DR}/r_{DC} = 3.00, 1.81, 1.16$ for intervals I, II and III, respectively). Such differences can potentially be used for

identifying secondary connections to co-regulated genes, in the particular case the constant but incomplete suppression of DsRed transcript by the shRNA.

We also look for similar defining features following a network reconstruction process with N = 60 as a resampling rate (Supplement Figure 4). The changes in confidence interval due to the smaller resampling rate do not affect our reconstruction conclusions. We also discover that selecting this confidence interval has negligible effect on the observed median values. Lastly, it is worth mentioning that the reconstruction results for the three different interval pairs (Figure 3b) point to the possibility of using a "consensus-based reconstruction". Under this strategy the consensus graph would consist of the significant connections that appear most of the times. This strategy yields a perfect reconstruction for our benchmark architecture (Supplement Figure 5).

Network reconstruction using mRNA measurements

We proceeded with mRNA measurements using qRT-PCR and performed the network reconstruction in a similar fashion. We performed titration of doxycycline and morpholino on cells harboring the benchmark circuit, but this time harvested the total mRNA of each population 48 hours after induction instead of directly measuring the fluorescence (Figure 4a). The perturbation intervals are also defined in the same fashion, with each Roman numeral signifying logarithmic increase in doxycycline and linear increase in morpholino from different starting points. We performed qRT-PCR to measure mRNA levels of each fluorescent protein and compared their relative values by using $\Delta\Delta C_t$ method with expression of GAPDH as the normalization factor for each gene. In this case we assume a Gaussian distribution for the biological triplicates of threshold cycle readings, and we employed Monte Carlo simulations to generate the confidence interval associated with each response coefficient. In these simulations, we draw random instances of $\Delta\Delta C_t$ values from a simulated normal distribution with mean and standard deviation identical to that of corresponding values obtained from three biological replicates. The simulated value is then used to calculate the global response coefficient in the same fashion as we did using flow cytometry data, by calculating the fractional change $\Delta ln(x_i)$ where x_i is the normalized copy number of mRNA. After performing 1,000 replicates of the simulation, we once again plotted the distribution on a boxplot showing 2.5 and 97.5 percentile of the data and display the reconstruction results with median response coefficient (Figure 4b).

The plot of relative mRNA copy number versus doxycycline and morpholino concentration shows a trend consistent with that of the dose-dependent response of protein expression; both AmCyan and DsRed are up-regulated in response to doxycycline, while only DsRed is sensitive to changing morpholino concentration. As a consequence, we observe that overall reconstruction results of two different types of data share a common trend of increased sensitivity as pre-perturbation concentration decreases, albeit with increased uncertainty due to standard deviation associated with $\Delta\Delta C_t$ calculation. Of the 6 non-zero edges (r_{DC} and r_{DR} from I and II and r_{MR} from IV and V) that were identified as accurate based on confidence interval derived from flow cytometry data (Figure 3b), only 2 of the corresponding edges (r_{DR} and r_{MR} from intervals I and IV, respectively) derived from qPCR data fit this criteria (Figure 4b). It is worth noting that, of the 4 that remain inconclusive, r_{DC} from interval I and r_{DR} from interval II was closest to being conclusive, with $P(r_{ij} > 0) = 0.958$ and 0.969, respectively (0.975 is the minimum requirement).

In order to examine further the noise associated with mRNA measurements, we performed a triplicate measurement of a benchmark cellular component via qRT-PCR. We chose the housekeeping gene GAPDH (also used for our qRT-PCR data normalization). After calculating the standard error of its expression among three separate experiments, we obtained the standard error to be 4.5%, a rate comparable to that of flow cytometry

experiments, but smaller than that of the AmCyan and DsRed mRNA measurements. Therefore, we anticipate that it is possible (e.g. primer selection and experimental repeats) to reduce the error in qRT-PCR measurements and potentially improve the decisiveness of the reconstruction results.

A difference between the protein and mRNA experiments is that the reverse engineering is applied to a gated population for the former while we use RNA harvested from all cells for the latter. Therefore, we hypothesize that we can improve the qRT-PCR based RE results by appropriately sorting a population of cells. Accordingly, we chose a pre- and post-perturbation interval most likely to result in decisive reconstruction results (intervals I and IV of Figure 3), and sorted the cells prior to the mRNA harvesting. We used the same criteria as we did in gating flow cytometry measurement (Supplement Figure 6). We then proceeded with qRT-PCR and subsequent network reconstruction. The newly recovered topology confirmed our hypothesis, successfully predicting signs all of the expected interactions with 95% confidence (Figure 4c). This was also reflected in our calculation of relative mRNA copy number analysis using $\Delta\Delta C_t$ calculation.

Conclusion

One of the main challenges in validating a biological network inference algorithm lies in defining suitable “ground truth” experiments. Traditionally, this task involved verification against known data[24, 25, 26] or using in silico simulations[27, 28, 29] which restricts possible tests and makes comparison across methods non-trivial. In this study, we show that genetic circuits integrated in human cells can serve as a benchmark for reverse engineering validation. After stably integrating a synthetic circuit with three different connections in human cells, we used a simple reverse engineering approach and were able to assess its performance in two different fronts: evaluation of reconstructed network based on defining features of the network, and comparison of reconstruction results using different species to represent the synthetic network activity. We chose to utilize protein and mRNA as the two representative species, and took steps to determine the appropriate statistical procedure for each measurement in order to increase the prediction confidence. Although both flow cytometry and qPCR data reflect defining features of the network, we had to tailor our analysis for each data type in order to obtain a coherent reconstruction result with reasonable confidence.

A critical issue with our reconstruction results was the inability to pick up statistically significant connections due to noise. While stochasticity is an inherent part of synthetic biological systems, other issues associated with transgenes–such as leakiness of expression and unwanted epigenetic silencing–are obstacles that limit their functions and utility for reverse engineering validation. In fact, the difficulties in using transgenic expression data for reverse engineering purpose has been highlighted by the second DREAM challenge, where majority of the state-of-the-art reverse engineering algorithms failed to reliably reconstruct a yeast synthetic gene network[30, 31, 32]. Perhaps, the most promising aspect of this study is its contribution towards unraveling previously unknown endogenous signaling and disease-related networks. Unraveling biological networks is central to understanding biology in general and human biology in particular. Many human diseases are essentially network-level phenomena. While engineering a large representative set of small to medium scale synthetic circuits in mammalian cells is a daunting task[33, 34], we argue that a few well-characterized circuits can be instrumental towards improving the theory and algorithms. We hope that eventually the validated RE methods will lead to the improvement in understanding and treating human diseases.

Materials and Methods

Bootstrap

For a standard calculation of experimental error several empirical measurements are averaged. If the probability density of the individual measurements has finite moments, then the true average is a t-distributed random variable with mean equal to the sample mean and standard deviation equal to the sample standard deviation divided by the square root of the number of samples (called the standard error). The 95% confidence interval means that the probability is less than 5% that the true value of the average lies more than 1.96 standard deviations from the sample mean. Bootstrapping is used to estimate the confidence interval for experiments where the t-distribution does not apply, or can't be assumed. For a simple example of bootstrapping, suppose that one is interested in estimating the median of a set of experimental replicates. Then a number of these replicates are drawn at random with replacement (i.e. replacing each number after each draw), the median is calculated, and this is repeated several times to obtain a distribution of medians. Then the 95% confidence interval of the true median is the range from the 2.5th to 97.5th percentile of the set of medians. In the main text we use bootstrapping to estimate the experimental error for the global response coefficients.

Stable transfection and cell line

The synthetic gene circuit construct was stably integrated into a HEK293 cell line using Flp-In 293 System (Invitrogen) according to the manufacturer's instructions. The cells were maintained at 37°C, 100% humidity and 5% CO_2. The complete growth medium consists of Dulbecco's modified Eagle's medium (Invitrogen) supplemented with 10% Fetal Bovine Serum (Invitrogen), 0.1 mM MEM non-essential amino acids (Invitrogen), 0.045 units/mL of Penicillin and 0.045 units/mL of Streptomycin (Invitrogen). Hygromycin B (Invitrogen) at 50 μg/ml was added as a selection agent. When the culture reached 75~90% confluency, it was passed first by washing with PBS (Mediatech), then trypsinized with 0.25% Trypsin-EDTA (Invitrogen). New culture was plated at 40% seeding density.

Fluorescence microscopy

Fluorescence images of live cells were captured 48–56 hours post-perturbation with doxycycline and morpholino. The live cells were grown on 12-well plates (Greiner Bio-One) in the complete medium. Cells were imaged using the Olympus IX81 microscope and a Precision Control environmental chamber. The images were captured using a Hamamatsu ORCA-03 Cooled monochrome digital camera. The filter sets (Chroma) are as follows: ET436/20x (excitation) and ET480/40m (emission) for AmCyan, ET560/40x (excitation) and ET630/75m (emission) for DsRed. Data collection and processing was performed in software package Slidebook 5.0. All images within a given experimental set were collected with the same exposure times and underwent identical processing.

Flow cytometry

For FACS experiment, cells were prepared as follows: 48 hours after perturbation, cells were trypsinized with 0.3ml of 0.25% trypsin-EDTA for 3 minutes and pelleted by centrifugation at 4000 rpm for 2 minutes. The pellet was resuspended with 0.4 ml of PBS (Mediatech). Analysis was performed with BD LSRFortessa. AmCyan protein was detected with a 445nm laser and a 515/20 band-pass filter, DsRed with a 561-nm laser, 610 emission filter and 610/20 band-pass filter. For each culture representing different conditions, 100,000 events were collected. Subsequent gating and analysis of the flow cytometry data was performed in FlowJo (Treetstar, Ashland, OR). For sorting, sample preparation was performed the same, but the analysis and sorting were performed with a BD FACSAria cell

sorter. For each condition, 200,000 cells that fell within the defined gate were collected as sorted population.

Quantitative RT-PCR

48 hours after perturbation, total RNA of the population was harvested using the RNeasy Mini kit (Qiagen) according to manufacturer's suggestion. 1 μg of total RNA was reverse transcribed to cDNA using QuantiTect Reverse Transcription kit (Qiagen). Quantitative PCR assays were performed with the Mastercycle ep realplex thermal cycler (Eppendorf) using the KAPA SYBR FAST qPCR kit (KAPA Biosystems). The relative mRNA expression levels of each node in the synthetic gene circuit were quantified with $\Delta\Delta C_t$ method, using GAPDH as normalization factor. Forward primer used to amplify GAPDH sequence was 5'-AATCCCATCACCATCTTCCA-3' and the reverse primer was 5'-TGGACTCCACGACGTACTCA-3'. Amplification started with an enzyme activation step at 95°C for 3 minutes, followed by 45 cycles consisting of 3 seconds of denaturation step at 95°C and 20 seconds of annealing/extension at 60°C.

Resampling rate selection

For proteins AmCyan and DsRed, we calculated the standard errors of 6.5% and 4.4%, respectively (Supplement Table 1). The 95% confidence interval of the mean is defined as $\bar{x} \pm (SE * 1.96)$, and by substituting SE with the observed value we can determine the limits of 95% confidence interval. For example, the observed standard error of 4.4% translates to $\bar{x} \pm 8.8\%$. In other words, the 'radius' of the 95% confidence interval (distance from mean to upper and lower boundary) in this case should be approximately 0.09 for the calculated global response coefficients. Supplementary Figure 3, the calculated global response coefficients vs. resampling rate (N), illustrates that increasing the resampling rate decreases the 95% confidence interval at a rate of $1/\sqrt{N}$. Therefore, N = 120 gives us a confidence interval radius of 0.09 ($1/\sqrt{120}=0.0912$).

Supplementary Material

Refer to Web version on PubMed Central for supplementary material.

Acknowledgments

This work was funded by the US National Institutes of Health (NIH) grant R21GM098984, TxACE SRC grant P12095, and the University of Texas at Dallas. We would like to thank Yi Li and Richard Moore for discussions.

References

1. Kholodenko B, Yaffe MB, Kolch W. Computational approaches for analyzing information flow in biological networks. Sci. Signal. 2012; 5:re1. [PubMed: 22510471]
2. Marbach D, Prill RJ, Schaffter T, Mattiussi C, Floreano D, Stolovitzky G. Revealing strengths and weaknesses of methods for gene network inference. Proc. Natl. Acad. Sci. U. S. A. 2010; 107:6286–6291. [PubMed: 20308593]
3. Sprinzak D, Elowitz MB. Reconstruction of genetic circuits. Nature. 2005; 438:443–448. [PubMed: 16306982]
4. Bansal M, Belcastro V, Ambesi-Impiombato A, di Bernardo D. How to infer gene networks from expression profiles. Mol. Syst. Biol. 2007; 3:78. [PubMed: 17299415]
5. Albert R, Dasgupta B, Sontag E. Inference of signal transduction networks from double causal evidence. Methods Mol. Biol. 2010; 673:239–251. [PubMed: 20835804]

6. Marbach D, Costello JC, Kuffner R, Vega NM, Prill RJ, Camacho DM, Allison KR, Kellis M, Collins JJ, Stolovitzky G. Wisdom of crowds for robust gene network inference. Nat Meth. 2012; 9:796–804.
7. Prill RJ, Marbach D, Saez-Rodriguez J, Sorger PK, Alexopoulos LG, Xue X, Clarke ND, Altan-Bonnet G, Stolovitzky G. Towards a rigorous assessment of systems biology models: The DREAM3 challenges. PLoS One. 2010; 5:e9202. [PubMed: 20186320]
8. Prill RJ, Saez-Rodriguez J, Alexopoulos LG, Sorger PK, Stolovitzky G. Crowdsourcing network inference: The DREAM predictive signaling network challenge. Sci. Signal. 2011; 4:mr7. [PubMed: 21900204]
9. Stolovitzky G, Monroe D, Califano A. Dialogue on reverse-engineering assessment and methods: The DREAM of high-throughput pathway inference. Ann. N.Y. Acad. Sci. 2007; 1115:1–22. [PubMed: 17925349]
10. He F, Balling R, Zeng AP. Reverse engineering and verification of gene networks: Principles, assumptions, and limitations of present methods and future perspectives. J. Biotechnol. 2009; 144:190–203. [PubMed: 19631244]
11. Cantone I, Marucci L, Iorio F, Ricci MA, Belcastro V, Bansal M, Santini S, di Bernardo M, di Bernardo D, Cosma MP. A yeast synthetic network for in vivo assessment of reverse-engineering and modeling approaches. Cell. 2009; 137:172–181. [PubMed: 19327819]
12. Kholodenko BN, Kiyatkin A, Bruggeman FJ, Sontag E, Westerhoff HV, Hoek JB. Untangling the wires: A strategy to trace functional interactions in signaling and gene networks. Proceedings of the National Academy of Sciences of the United States of America. 2002; 99:12841–12846. [PubMed: 12242336]
13. Sontag ED. Network reconstruction based on steady-state data. Essays Biochem. 2008; 45:161–176. [PubMed: 18793131]
14. Kholodenko BN. Untangling the signalling wires. Nat. Cell Biol. 2007; 9:247–249. [PubMed: 17330115]
15. Sontag E, Kiyatkin A, Kholodenko BN. Inferring dynamic architecture of cellular networks using time series of gene expression, protein and metabolite data. Bioinformatics. 2004; 20:1877–1886. [PubMed: 15037511]
16. Santos SD, Verveer PJ, Bastiaens PI. Growth factor-induced MAPK network topology shapes erk response determining PC-12 cell fate. Nature cell biology. 2007; 9:324–330.
17. Bruggeman FJ, Westerhoff HV, Hoek JB, Kholodenko BN. Modular response analysis of cellular regulatory networks. J. Theor. Biol. 2002; 218:507–520. [PubMed: 12384053]
18. Gossen M, Freundlieb S, Bender G, Muller G, Hillen W, Bujard H. Transcriptional activation by tetracyclines in mammalian cells. Science. 1995; 268:1766–1769. [PubMed: 7792603]
19. Bleris L, Xie Z, Glass D, Adadey A, Sontag E, Benenson Y. Synthetic incoherent feedforward circuits show adaptation to the amount of their genetic template. Molecular Systems Biology. 2011; 7
20. Rinaudo K, Bleris L, Maddamsetti R, Subramanian S, Weiss R, Benenson Y. A universal RNAi-based logic evaluator that operates in mammalian cells. Nat. Biotechnol. 2007; 25:795–801. [PubMed: 17515909]
21. Summerton J, Weller D. Morpholino antisense oligomers: Design, preparation, and properties. Antisense Nucleic Acid Drug Dev. 1997; 7:187–195. [PubMed: 9212909]
22. Choi WY, Giraldez AJ, Schier AF. Target protectors reveal dampening and balancing of nodal agonist and antagonist by miR-430. Science. 2007; 318:271–274. [PubMed: 17761850]
23. Efron, B.; Tibshirani, RJ. An Introduction to the Bootstrap. 1st ed. Chapman & Hall/CRC; 1993.
24. Sachs K, Perez O, Pe'er D, Lauffenburger DA, Nolan GP. Causal protein-signaling networks derived from multiparameter single-cell data. Science. 2005; 308:523–529. [PubMed: 15845847]
25. Xu TR, Vyshemirsky V, Gormand A, von Kriegsheim A, Girolami M, Baillie GS, Ketley D, Dunlop AJ, Milligan G, Houslay MD, Kolch W. Inferring signaling pathway topologies from multiple perturbation measurements of specific biochemical species. Sci. Signal. 2010; 3:ra20.
26. Pe'er D, Hacohen N. Principles and strategies for developing network models in cancer. Cell. 2011; 144:864–873. [PubMed: 21414479]

27. Dalle Pezze P, Sonntag AG, Thien A, Prentzell MT, Godel M, Fischer S, Neumann-Haefelin E, Huber TB, Baumeister R, Shanley DP, Thedieck K. A dynamic network model of mTOR signaling reveals TSC-independent mTORC2 regulation. Sci. Signal. 2012; 5:ra25. [PubMed: 22457331]

28. Marbach D, Schaffter T, Mattiussi C, Floreano D. Generating realistic in silico gene networks for performance assessment of reverse engineering methods. J. Comput. Biol. 2009; 16:229–239. [PubMed: 19183003]

29. Basso K, Margolin AA, Stolovitzky G, Klein U, Dalla-Favera R, Califano A. Reverse engineering of regulatory networks in human B cells. Nat. Genet. 2005; 37:382–390. [PubMed: 15778709]

30. Stolovitzky G, Prill RJ, Califano A. Lessons from the DREAM2 Challenges. Ann. NY Acad. Sci. 2009; 1158:159–195. [PubMed: 19348640]

31. Marbach D, Mattiussi C, Floreano D. Replaying the evolutionary tape: biomimetic reverse engineering of gene networks. Ann. N.Y. Acad. Sci. 2009:1465.

32. Baralla A, Mentzen W, De La Fuente A. Inferring gene networks: dream or nightmare? Part 1: Challenges 1 and 3. Ann. N.Y. Acad. Sci. 2009:1465.

33. Yokobayashi Y, Weiss R, Arnold FH. Directed evolution of a genetic circuit. Proc Natl Acad Sci U S A. 2002; 99(26):16587–16591. [PubMed: 12451174]

34. Ellis T, Wang X, Collins JJ. Diversity-based, model-guided construction of synthetic gene networks with predicted functions. Nat Biotechnol. 2009; 27(5):465–471. [PubMed: 19377462]

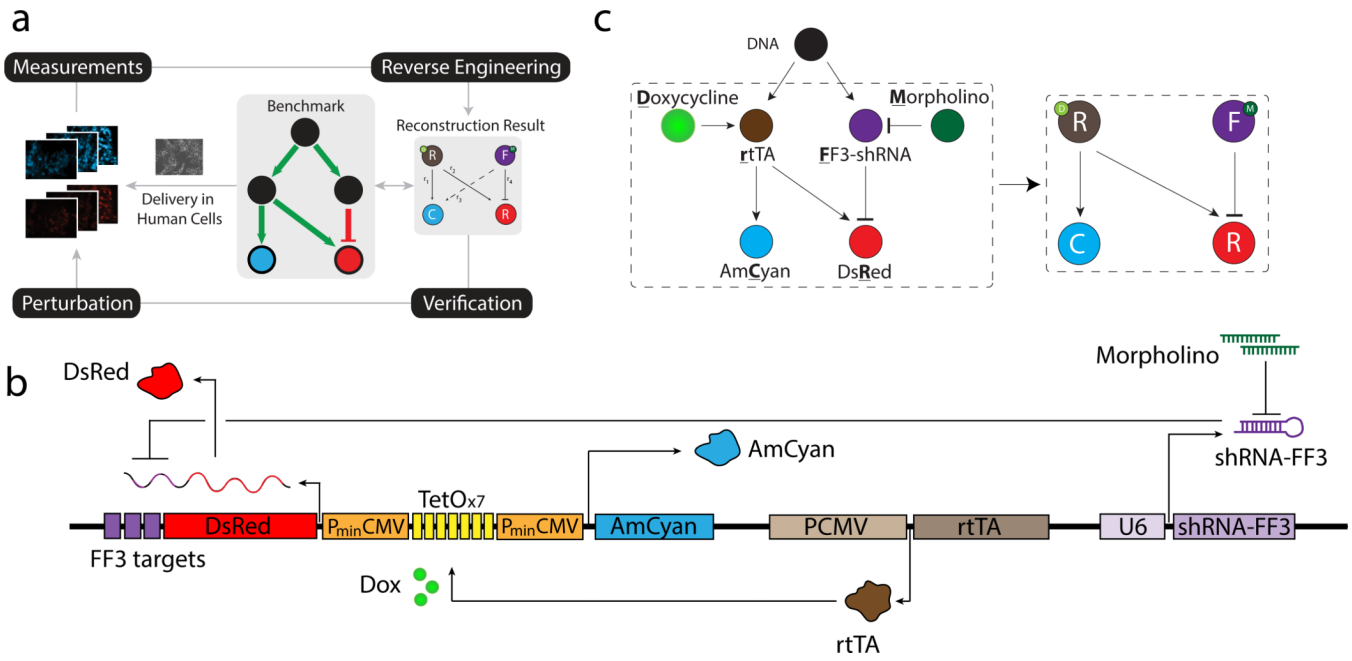

Figure 1. A platform for assessment of reverse engineering using a synthetic circuit

(a) A workflow diagram of the proposed platform. The benchmark architecture is stably integrated in a human cell line. A reverse engineering algorithm undergoes validation using perturbations and by verifying the results using the benchmark. **(b)** The synthetic circuit delivered to human embryonic kidney cells using FLP recombinase-mediated stable integration (Flp-In). In the presence of doxycycline, a constitutively transcribed reverse tetracycline-induced transactivator (rtTA) induces transcription of both fluorescent proteins by binding to the tetO enhancer region of the bidirectional promoter. A short-hairpin RNA, which is also constitutively transcribed, actively represses translation of DsRed by binding to the target sequence present in 3' UTR of the DsRed mRNA transcript. Addition of a morpholino oligo reduces the shRNA activity by protecting the 3' UTR target site of the shRNA. **(c)** A diagram depicting the benchmark synthetic gene circuit. The circuit consists of two distinct regulatory elements with different mechanisms to control the expression levels of AmCyan and DsRed fluorescent proteins.

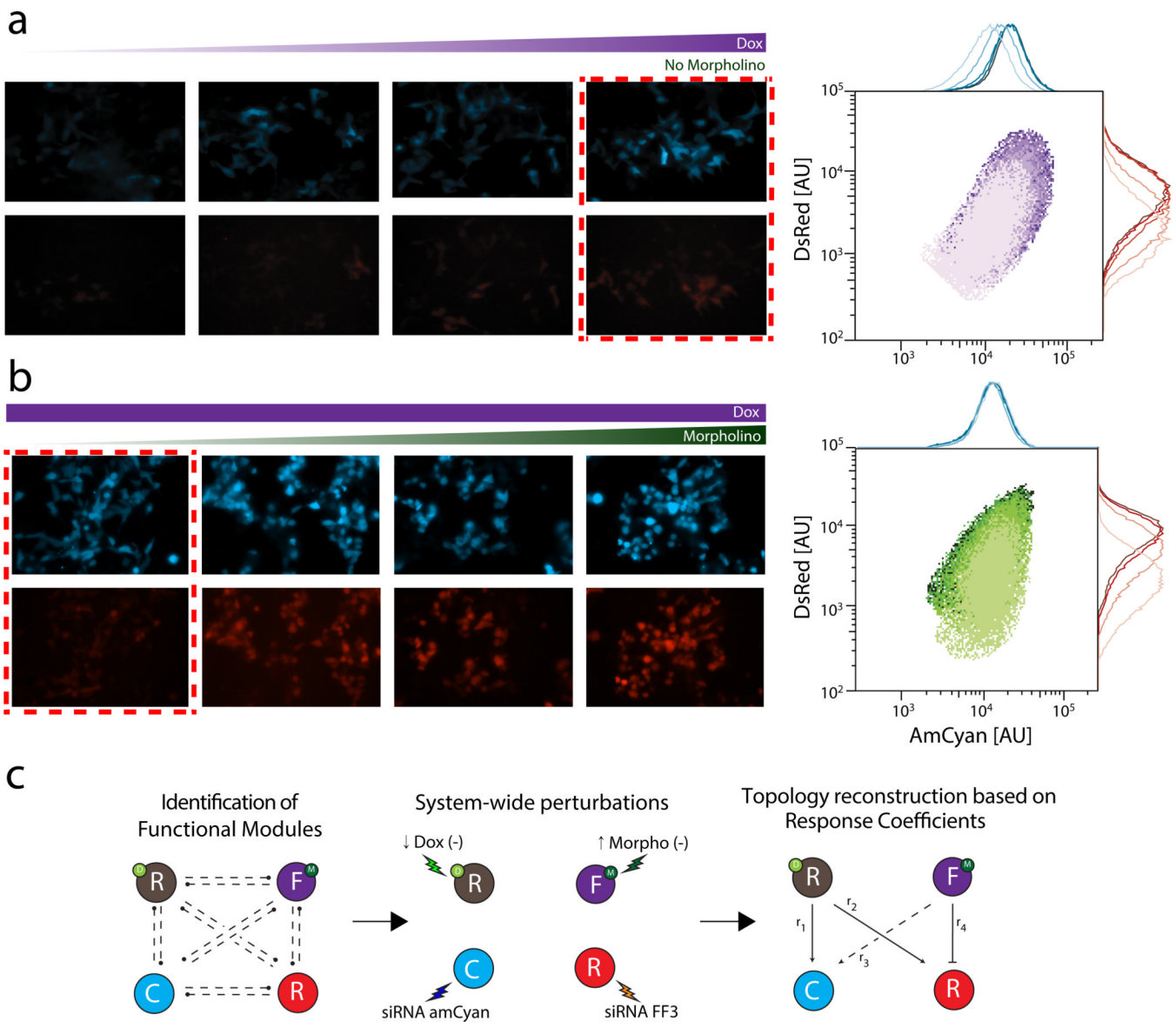

Figure 2. Characterization experiments

(a) Fluorescence microscopy and gated flow cytometry results of doxycycline titration in the absence of morpholino. **(b)** Fluorescence microscopy and gated flow cytometry results of morpholino titration for fixed saturated doxycycline concentration. Doxycycline concentration ranged from 1 ng/ml to 10 μg/ml, while morpholino concentration ranged from 0 to 5 nmol/ml. Images surrounded by red box shows identical condition: 10 μg/ml doxycycline and 0 nmol/ml morpholino. **(c)** Schematic representation of modular response analysis. Semi-quantitative sensitivity analysis is performed by applying systematic perturbations to each modular component. The resulting change in activity of each module is determined as global response coefficient.

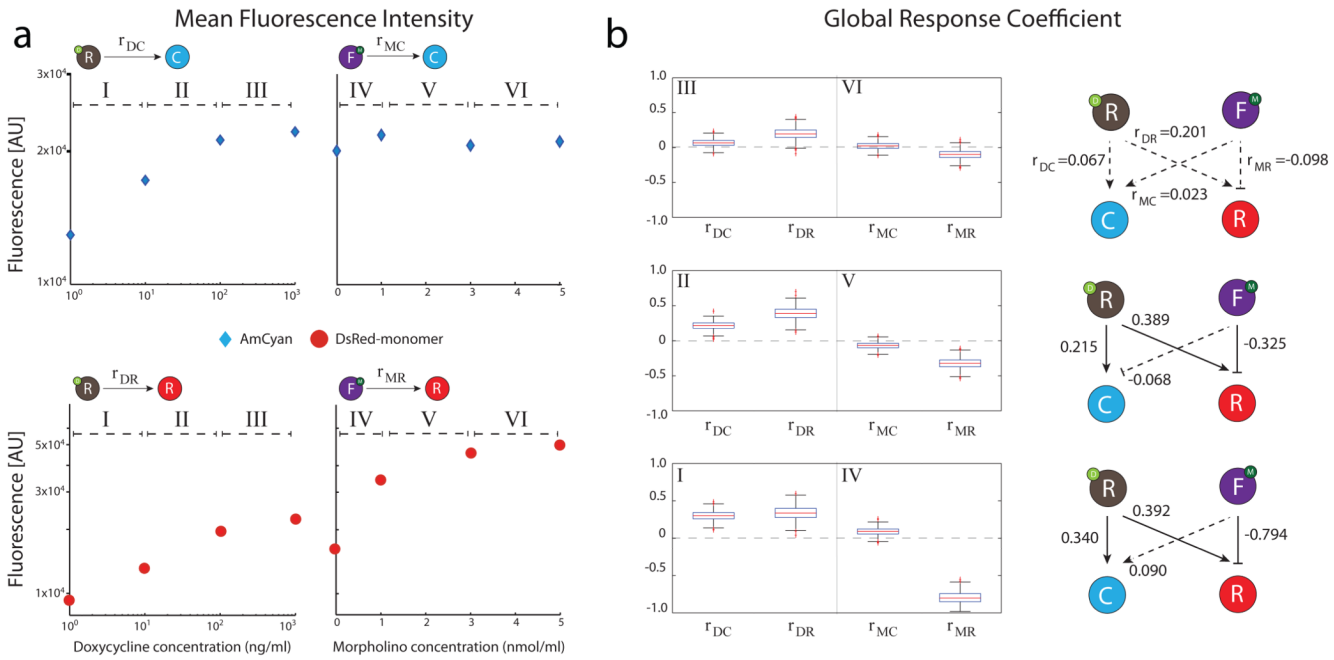

Figure 3. Reverse engineering using flow cytometry protein measurements

(a) Cells harboring the synthetic circuit construct were perturbed with various concentrations of doxycycline and morpholino. After 48 hours of induction, cells were harvested and their expression of AmCyan and DsRed are measured via fluorescence using flow cytometry (n ≥ 100,000). After gating of flow cytometry results to include only the cells responsive to chemical perturbations (n' ≥ 10,000), mean of AmCyan and DsRed fluorescence is plotted as a function of doxycycline and morpholino concentration. The Doxycycline titration was performed while keeping morpholino at 0 nmol/ml and morpholino titration was performed with doxycycline concentration of 10 μg/ml. To simulate different perturbation conditions, each step-wise change in chemical concentration is defined as intervals I–VI. **(b)** Global response coefficient of a given interval. Bootstrap resampling method is used to obtain the confidence interval of the response coefficients. For the resampling method, 120 random cells are drawn from pre-and post-perturbation, and their average is used to calculate the response coefficient. Such calculation is performed 1,000 times, and the result is shown as a boxplot showing 95% confidence interval (whiskers). Red + indicates outliers. Networks on the right show complete network reconstruction results. Values denote the median response coefficient confidence interval. Dotted lines represent cases where the 95% confidence interval of the corresponding obtained from simulation includes zero, whereas solid lines indicate cases where it does not.

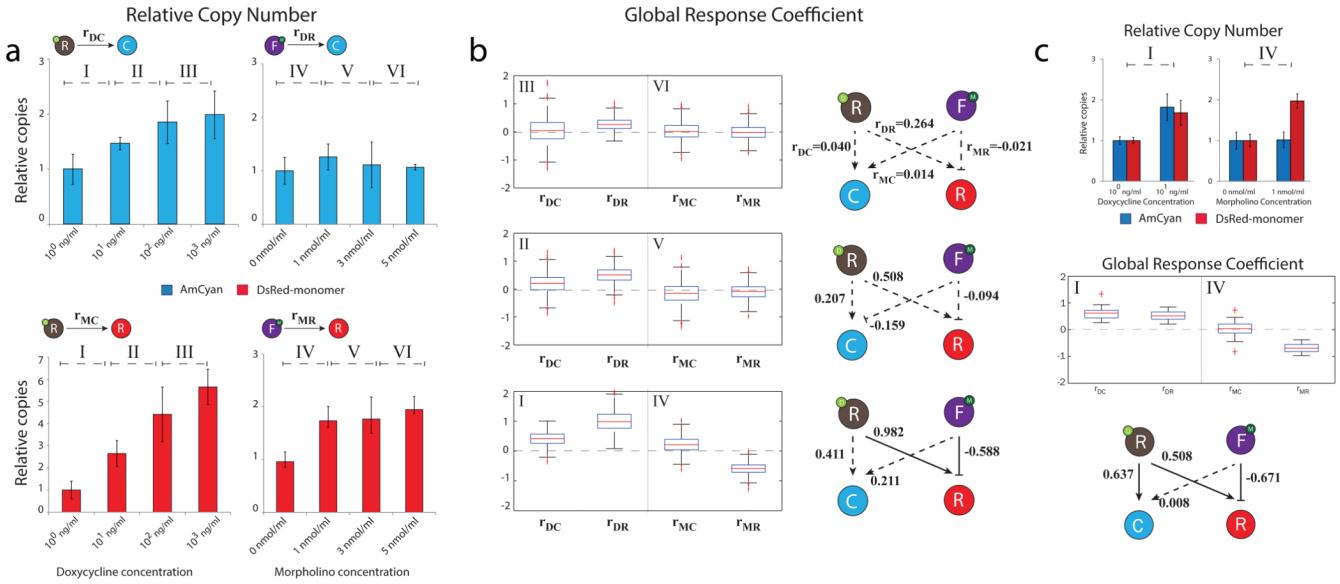

Figure 4. Reverse engineering using qRT-PCR mRNA measurements

(a) Cells stably integrated with the synthetic circuit were perturbed with various concentrations of doxycycline and morpholino. Total mRNA was extracted 48 hours post-induction, and relative abundance of fluorescent output mRNA was measured using qRT-PCR with $\Delta\Delta C_t$ method. The data shown consists of three separate experiments with each with triplicate PCR results, and error bars indicate standard error of the mean. Each step-wise decrease in perturbation agent is labeled as a single interval (denoted by Roman numerals) to simulate perturbation conditions for acquisition of response coefficients. **(b)** Global response coefficients of each simulated perturbation interval. To quantify the accuracy of the result, Monte Carlo simulation was used to build a confidence interval of the response coefficients. The results are displayed as boxplots showing 95% confidence intervals (whiskers). Networks on the right shows complete network reconstruction results. Values denote the median response coefficient confidence interval. Dotted lines represent cases where the 95% confidence interval of the corresponding obtained from simulation includes zero, whereas solid lines indicate cases where it does not. **(c)** Cells grown in pre- and post-perturbation intervals I and IV were sorted for high fluorescence using FACS prior to extracting mRNA. Harvested mRNA of the selected population was then used for qRT-PCR (top) and subsequent network reconstruction (bottom) as in (b).